ACS NANO

www.acsnano.org

ARTICLE

Concentrated Near-Field Thermoradiative Device Approaching Solar Cell Performance at Nighttime

Dudong Feng* and Xiulin Ruan*

Cite This: *ACS Nano* 2025, 19, 17357−17364

Read Online

ACCESS | Metrics & More | Article Recommendations | Supporting Information

ABSTRACT: **Thermoradiative (TR) cells operate by harnessing the outgoing thermal radiation from Earth to outer space to extract work. Despite recent advancements in nighttime power generators, TR technology faces challenges with low output power and efficiency, falling far less than its theoretical limits. In this letter, we investigate the key limiting factors affecting performance metrics. By introducing a near-field atmosphere coupler composed of a polar dielectric absorber and a concentrated thermal emitter with optimized parameters, the maximum output power could be boosted to 180 W/m^2 with a 20-fold increase in the emission area, approaching the level of solar panels. Additionally, we explore material selection and integration strategies to showcase the feasibility and challenges of this technology. Our findings indicate that, analogous to the role of concentrated solar power in the solar power landscape, this technology could herald an emerging frontier for researchers in the field of renewable energy generation.**

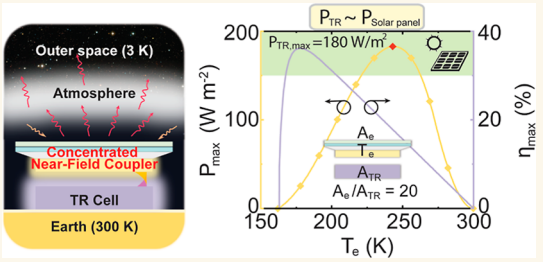

KEYWORDS: *nighttime electricity generation, concentrated thermoradiative, radiative cooling, near-field radiation, polar dielectric, surface phonon-polaritons*

INTRODUCTION

From a thermodynamic perspective, the earth can be seen as an isolated system with energy conservation between two reservoirs: the sun at 5700 K and the deep space at 3 K. Noteworthily, people have developed numerous technologies that utilize solar power to sustain human society, with silicon-based solar panels playing a significant role in electrifying the daily lives of human beings.[1,2] According to the first law of thermodynamics, all absorbed solar power by the Earth should be emitted as thermal radiation, predominantly in the mid-infrared spectrum. The atmospheric window's high transparency in the range of 8−13 μm facilitates significant thermal radiation from the Earth's surface to outer space.[3,4] Leveraging this outgoing thermal radiation, a heat engine can extract work from this heat flow.[5−8] Given these principles, the foundation of nighttime power generation is well established and coherent. Furthermore, harnessing renewable energy during nighttime complements daytime off-grid energy generation, which significantly enhances electric-grid stability, helps mitigate energy crises, and contributes to the alleviation of global warming.[9−11]

Two primary technology pathways for nighttime power generation are thermoradiative (TR) technology and radiative-cooling-based energy generators. A TR cell, initially introduced as an emissive energy harvester by Byrnes,[6] is capable of directly producing electricity through a negative illumination into outer space during nighttime.[12] Through thermal-driven carrier diffusion processes, a semiconductor pn diode can generate a positive electric current under a negative applied bias voltage, effectively counterbalancing the rate between generation and radiative recombination.[12,13] This process ultimately yields net useful work from the system.[14] Several recent works have experimentally demonstrated this concept,[12,15] nonetheless, with limited output power (∼2 mW/m^2) and efficiency (∼1%).[16] Leveraging decades of research on radiative cooling[17−23] and recent advancements in daytime subambient radiative cooling technology,[24−31] radiative cooling thermoelectric (RC-TE) generators have garnered significant attention over the past few years.[32−37] Typically, a thermoelectric generator is positioned between a local heat source and the cold reservoir facilitated by radiative cooling. Since this concept was implemented, the state of the art has reached 100 mW/m^2 of

Received: November 15, 2024
Revised: April 1, 2025
Accepted: April 2, 2025
Published: April 30, 2025

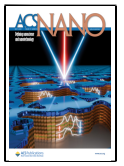

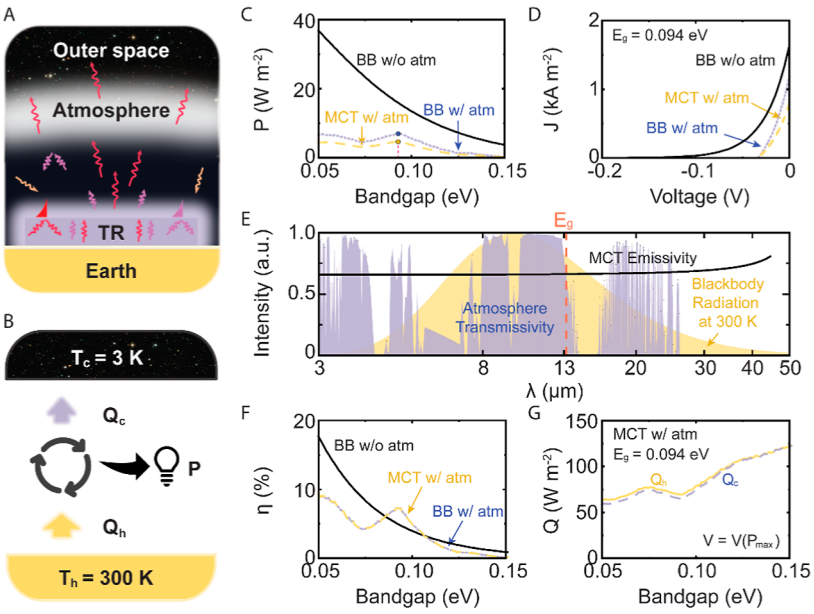

Figure 1. Performance of a conventional TR cell. (A) The schematic of a conventional TR cell working at nighttime. (B) The energy flow scheme of a conventional TR cell. Q_h, Q_c, and P represent the absorbed energy from the earth, the dissipated heat to outer space, and the generated power from the TR cell, respectively. Unless specified in context, the Earth and TR cell (T_h) is assumed to be 300 K, and the temperature of outer space (T_c) is assumed to be 3 K. (C) The maximum power of a TR cell with respect to the bandgap with three different configurations: blackbody TR cell without atmospheric absorption, blackbody TR cell with atmospheric absorption, and a MCT TR cell with atmospheric absorption. (D) The current−voltage curve of these three TR configurations. (E) The emissivity of MCT, the transmissivity of the atmosphere, and the blackbody radiation at 300 K. (F) The maximum efficiency with respect to the bandgap of TR cells. (G) The absorbed energy (Q_h) and dissipated heat (Q_c) of the MCT TR cell with respect to the bandgap. The environment temperature is set to 300 K as default unless specified in the context.

the thermoelectric generator area.[37] However, it is important to note that the theoretical upper limit of a TR cell output power is orders of magnitude higher than that of a RC-TE device.[15,38] This highlights substantial room for performance enhancements of TR technology.

The fundamental thermodynamic limit of a single TR cell could potentially reach up to 48.4 W/m^2 under the assumption of blackbody radiation.[5] However, considering the intrinsic characteristics of an ideal semiconductor and the realistic transmissivity of the atmospheric window, the maximum output power is substantially lower. In a manner akin to the enduring queries within the solar cell industry, the following questions are introduced here: what are the key factors that impact the performance of a TR cell? How can we push this technology to approach the blackbody limit and even achieve output power comparable to that of a solar panel? In this letter, we will systematically address these two questions. First, we perform a detailed balance analysis to identify all the factors influencing the performance of a standard HgCdTe (MCT) TR cell. Then, we propose a novel TR configuration featuring a near-field atmosphere coupler made of a polar dielectric absorber and a radiative cooling emitter, which is analogous to a solar near-field thermophotovoltaic device. Through the implementation of this design, the nighttime power generator achieves an impressive output power of 11.0 W/m^2, reaching approximately 91% of the output power generated by a Carnot engine. We further update the coupler to be a concentrated near-field atmosphere coupler to potentially boost the output power to 180 W/m^2 with a 20-fold increase in the emission area, which approaches the output power level of a single solar panel. Our theoretical prediction of concentrated near-field TR devices presents a promising avenue for nighttime power generation, serving as a parallel approach to existing renewable energy generation technologies and enriching the spectrum of carbon neutrality techniques.

RESULTS AND DISCUSSION

Performance Bottlenecks of Conventional TR Cells. Figure 1A shows the schematic of a conventional TR cell, which is usually made of a semiconductor diode. The photodiode would convert the heat absorbed from the earth to build up a negative bias that facilitates the flow of free charges to drive an external load within a wired loop. The thermal radiation and negative illumination due to the negative bias would be confined or reflected by the interface between the semiconductor and air, which can potentially hinge the energy flow. In addition, for a TR cell working on the Earth's surface, the existence of the atmosphere acts as a radiation shield that only allows light at certain wavelengths to dissipate heat into outer space. Essentially, the TR cell is a heat pump that works between the Earth and outer space reservoirs as shown in Figure 1B. The optical processes described above constitute the energy flow in this thermodynamic picture. To understand the key factor that affects the TR cell, we would assume the TR cell to be an ideal photodiode without any loss coming from nonradiative processes and charge transport. Employing a detailed balance analysis (see Methods), we could answer the first proposed question: what is the bottleneck of conventional TR technology?

We investigate two important factors that greatly deteriorate the performance of a conventional TR cell: the radiation shield effect due to atmospheric absorption and the total internal reflection due to a high refractive index of a narrow bandgap semiconductor. As shown by the black solid curve in Figure 1C, we recalculate the blackbody limit with an extension by including the effect of the bandgap. By taking into consideration

https://doi.org/10.1021/acsnano.4c16433
ACS Nano 2025, 19, 17357−17364

the atmospheric absorption, the maximum output power of the blackbody TR cell is reduced to 7.0 W/m^2 (shown as the blue point in Figure 1C), which is far below the blackbody limit (48.4 W/m^2) calculated in ref 5. Therefore, unless the TR cell operates in outer space, this blackbody limit with consideration of atmospheric absorption would be more practically significant for researchers to design a TR cell on Earth. Moreover, to give a more realistic estimation, we choose a MCT photodiode to replace the blackbody photodiode for its tunable bandgap. The maximum output power would further drop to 4.55 W/m^2 (shown as the yellow point in Figure 1C). For both the blackbody photodiode and MCT photodiode, the optimal bandgap corresponding to the maximum output power occurs at around 0.094 eV as the atmospheric window starts at approximately 13.2 μm, which aligns with the calculation in ref 15. The current−voltage characteristics of these three TR configurations are also plotted in Figure 1D. With the atmospheric absorption, both short-circuit current and open-circuit voltage decrease since fewer photons can be directly emitted into outer space. Nevertheless, replacing the blackbody photodiode with a MCT photodiode maintains the open-circuit voltage while reducing the short-circuit current by 33%. This is attributed to the total internal reflection resulting from the high refractive index of MCT, i.e., $n \approx 3.7$ in the sky window (8−13 μm). As shown in Figure 1E, the spectral hemispherical emissivity of MCT above the optimal bandgap is equal to 0.67, explaining the reduction in the maximum output power. The purple shaded region represents atmospheric transmissivity, while the yellow shaded region depicts blackbody radiation at 300 K. The overlapping area signifies thermal radiation that can be directly emitted into outer space. The dashed orange line in the figure represents the bandgap, dividing the overlapping area into two parts. The portion above the bandgap represents useful thermal radiation that can be extracted for electricity, while the part below the bandgap is considered waste heat, parasitically emitted as thermal radiation. The optimal bandgap occurs at around 13 μm, covering the conventional sky window for emission, which allows the outgoing thermal radiation to generate free charges with minimum thermalization and parasitic emissions.

Figure 1F shows the efficiency−bandgap (η−E_g) curves of three TR configurations. The η−E_g curve of the blackbody TR cell overlaps with the MCT TR cell, as the reduction due to the high refractive index of MCT affects the dissipated heat (Q_c) by the same ratio. Interestingly, the efficiency of the blackbody TR cell with atmospheric absorption surpasses that without atmospheric absorption in a certain bandgap range (0.086−0.107 eV). This suggests that TR cells could benefit from atmospheric absorption as it blocks some parasitic emission. However, the overall efficiency remains below 10%, which is low compared to the Carnot efficiency achievable between these two temperature reservoirs. We examined the absorbed energy and dissipated heat at the voltage corresponding to the maximum output power, i.e., $V = V(P_{max})$, as shown in Figure 1G. With increasing bandgap, both Q_h and Q_c rise, but less P is produced as more thermal radiation turns into parasitic emission. However, the maximum emissive power from the Earth to outer space is far more than Q_c, signifying that only partial emission power is harnessed to generate electricity using the conventional TR configuration.

TR Configuration with a Near-Field Polar Dielectric Absorber. A potential solution for boosting the performance of the conventional TR cells is to add a near-field absorber between the TR cells and outer space, as shown in Figure 2A. The bandgap of the TR cell and the material parameters of the polar

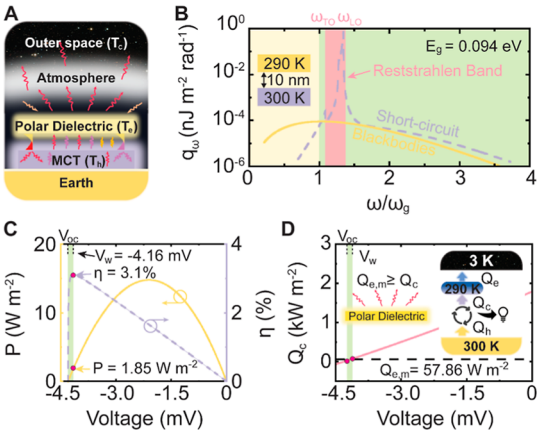

Figure 2. TR configuration with a near-field polar dielectric absorber. (A) The schematic of a near-field TR configuration with a polar dielectric that can absorb more photons than the blackbody limit from the TR cell at a desired spectrum. (B) The spectral heat flux of the near-field TR configuration (V = 0 V) and two blackbodies with the same temperatures. The yellow shaded area represents the parasitic thermal emission below the bandgap, and the green shaded area represents the thermal emission that can potentially produce free carriers. The pink shaded area is the Reststrahlen band, bounded by the transverse optical phonon (ω_{TO}) and the longitudinal optical phonon (ω_{LO}). The polar dielectric absorber (T_e) is fixed at 290 K. The thicknesses of the MCT TR cell (t_{TR}) and the polar dielectric absorber (t_{pd}) are 50 nm and 1 μm, respectively. The vacuum spacing distance (d) is fixed at 10 nm, and the bandgap of the MCT TR cell is chosen to be 0.094 eV as default unless specified. (C) The P−V and η−V curves of the near-field TR configuration. The green shaded area represents the operational area considering the dissipated heat limit of the polar dielectric. (D) The dissipated heat and emitted heat with respect to the voltage of the near-field TR configuration. The inserted plot shows the thermodynamic schematic of this configuration.

dielectric absorber have been optimized (see Methods). Placing the polar dielectric at a nanoscale vacuum gap with the TR cell allows the confined photon due to the high refractive index of MCT to be extracted through the photon tunneling effect. Moreover, through the spectral matching between the surface phonon-polaritons (SPhPs) of the polar dielectric absorber and interband transition of the MCT TR cell, the spectral heat flux can be enhanced by orders of magnitude higher than the blackbody limit, as shown in Figure 2B. The same mechanism has been applied to create novel nonlinear thermal components[39−41] and high-performance radiative energy converters.[13,42] The key benefit of this material selection and device is its ability to concentrate the spectral heat flux within the Reststrahlen band ($\omega_{TO} < \omega < \omega_{LO}$), allowing for selective extraction of useful photons near the bandgap from the MCT TR cell while the parasitic thermal emission and thermalization loss are minimized relatively. The output power and voltage (P−V) and efficiency and voltage (η−V) curves are shown in Figure 2C, although complete curves might be hard to achieve under this configuration. According to the thermodynamic picture of this configuration in Figure 2D, the dissipated heat of the MCT TR cell should equal the outgoing thermal emission of the polar dielectric absorber to satisfy the energy conservation law, i.e., $Q_e = Q_c$. Therefore, the dissipated heat should not exceed the

https://doi.org/10.1021/acsnano.4c16433
ACS Nano 2025, 19, 17357−17364

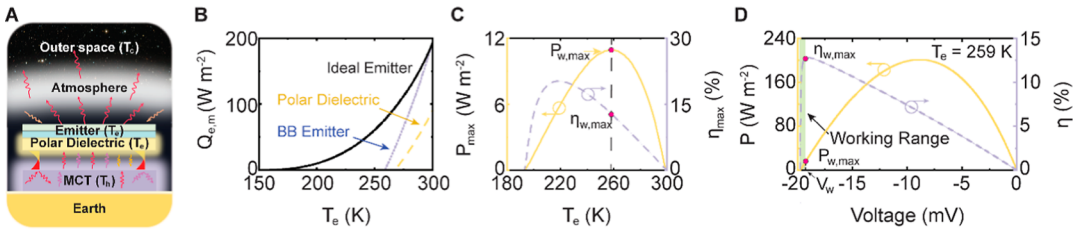

Figure 3. TR configuration with a near-field atmosphere coupler made of a polar dielectric absorber and a radiative cooling emitter. (A) The schematic of a near-field TR configuration with a polar dielectric and a radiative cooling emitter that can dissipate more heat into outer space. The temperature of the radiative cooling emitter is assumed to be the same as the polar dielectric absorber. (B) The maximum emissive power ($Q_{e,m}$) of three different thermal emitters: an ideal emitter, a blackbody emitter, and the optimized polar dielectric absorber with respect to the surface temperature. (C) The maximum output power and efficiency of this near-field TR configuration with respect to the emitter temperature. (D) The $P-V$ and $\eta-V$ curves of the near-field TR configuration with a radiative cooling emitter. The green shaded area represents the operational area.

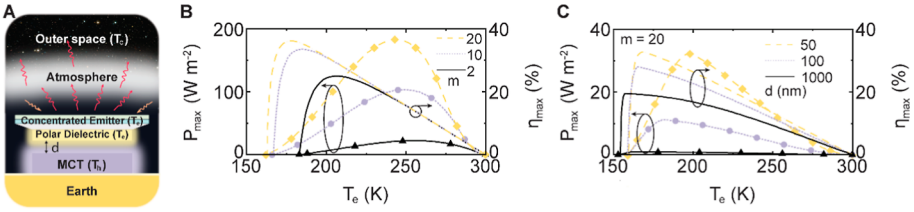

Figure 4. Concentrated TR configuration with a near-field atmosphere coupler. (A) The schematic of a near-field TR configuration with a polar dielectric and a concentrated radiative cooling emitter with an area m times that of the MCT TR cell. (B) The maximum output power and efficiency of this near-field TR configuration with respect to the emitter temperature at different concentration ratios with d = 10 nm. (C) The maximum output power and efficiency of this near-field TR configuration with respect to the vacuum gap distance at different vacuum gap distances with m = 20. Note that the power density is based on the TR cell area.

maximum capacity of the outgoing thermal emission by the polar dielectric absorber, i.e., $Q_{e,m} \geq Q_c$. Nonetheless, the polar dielectric absorber cannot serve as a good thermal radiation emitter because the sky window overlaps with the Reststrahlen band so that the emissivity is extremely low due to the highly mismatched impedance (the refractive index is almost zero). For instance, when T_e = 290 K, the maximum emissive power ($Q_{e,m}$) of this polar dielectric is only 57.86 W/m^2, while the dissipated heat of this MCT TR cell at short circuit (V = 0 V) is 1793.7 W/m^2. Therefore, the actual functioning curve of this near-field configuration is confined to the green shaded area in Figure 2D, considering the emission power limitations (from 0 to 57.86 W/m^2). The operational voltage (also shown in the green shaded area in Figure 2C) spans from the open-circuit voltage (V_{oc} = −4.30 mV) to the working voltage (V_w = −4.16 mV), with a maximum output power of 1.85 W/m^2 and a peak efficiency of 3.1%. Certainly, this near-field TR configuration cannot reach its full potential unless we enhance the emissive power limit.

TR Configuration with a Near-Field Atmosphere Coupler. To address the problem, here we proposed to coat a radiative cooling emitter on the polar dielectric absorber to enhance the heat dissipation as shown in Figure 3A. Considering the atmosphere is semi-opaque,[43] the spectral emissivity of the ideal emitter can be optimized according to the net radiative cooling power of the emitter.[38] In other words, we set the spectral emissivity to unity when the outgoing radiation exceeds the incoming radiation from the environment (including the atmosphere and outer space) and to zero otherwise (see Methods). As clearly shown in Figure 3B, at 300 K, the ideal emitter and blackbody emitter can achieve a maximum emissive power of 193.59 W/m^2, over twice the power of the polar dielectric absorber at 89.54 W/m^2, highlighting the need for integrating a spectrally designed radiative cooling emitter. Figure 3C shows the maximum output power and efficiency of this near-field TR configuration using the ideal emitter to dissipate the heat. The maximum output power and efficiency increase as the emitter temperature decreases due to the improvement in the $P-V$ curve with a larger temperature difference in the near-field TR device. However, as the emitter temperature continues to rise, the dissipated power decreases significantly, which limits further increases in output power. The optimal emitter temperature for maximum efficiency is lower than that for maximum output power because efficiency is less constrained by dissipated power. Therefore, at the optimal emitter temperature for output power (T_e = 259 K), this near-field TR configuration showcases a maximum output power of 11.0 W/m^2 (91% of Carnot output power) and a maximum efficiency of 12.6%. Although the emission temperature of this TR configuration is reduced by adding this coupler, both output power and efficiency are more than double the figures of a conventional TR cell and 1.6 times higher than those of a blackbody TR cell. To be noted, the maximum output power and the maximum efficiency cannot be achieved at the same time. Figure 3D displays the $P-V$ and $\eta-V$ curves of this near-field TR configuration when T_e = 259 K. Obviously, the near-field TR configuration has not fully realized its output power potential. The operational area (green shaded region) falls short of covering the peak value due to the emissive power limit.

Concentrated TR Configuration with a Near-Field Atmosphere Coupler. To further enhance the emissive power limit, we propose a thermally concentrated near-field TR configuration achieved by increasing the area ratio between the emitter and the TR cell, which we term the concentration ratio (m) to draw an analogy with concentrated solar technology, which has already been widely applied in radiative cooling[44−46] and thermoelectrics.[47] The schematic of this

https://doi.org/10.1021/acsnano.4c16433
ACS Nano 2025, 19, 17357−17364

concentrated near-field TR configuration is shown in Figure 4A. Assuming no convection or conduction leakage from the environment, the emissive power of this concentrated radiative cooling emitter can be linearly enhanced by the concentration ratio. With m = 20, Figure 4B indicates that this configuration can boost the maximum output power to exceed 180 W/m^2 at T_e = 244 K, which is remarkable as it approaches that of a conventional solar panel. This extraordinary output power does not violate the blackbody limit of negative illumination[5] as the unit area surface is defined as the TR cell, not the emitting surface. The enhancement ratio of the maximum output power is 16 times that of a regular radiative cooling emitter, and it is not proportional to the concentration ratio because the optimized material parameters of the polar dielectric are tailored for the emitter temperature fixed at 290 K, not at 244 K. Therefore, the increase in the maximum output power of the TR cell is not linearly related to the maximum emissive power. The peak efficiency can reach 36.2% with a lower emitter temperature. As detailed in the Supporting Information, even for a concentrated blackbody emitter (m = 20), the maximum output power can exceed 77 W/m^2, and the peak efficiency can reach 12.2% (Figure S1). For practical purposes, the recently developed ultrawhite radiative cooling paint,[25] which is easily scalable and cost-effective, can be used to mimic a blackbody emitter in the mid-IR range. Our evaluation of this practical configuration revealed results comparable to those of a blackbody emitter (Figure S2). Sure enough, aiming for better performance, we can further increase the concentration ratio. The theoretical limit of the TR performance is reached when the emitter temperature approaches infinitely close to the temperature of outer space. However, even with the best thermal insulation materials, there will still be heat leakage from the environment, which occupies the amount of useful heat available for electricity generation. Therefore, increasing the emitter surface area will eventually lead to diminishing returns in performance. In Figure 4C, we also investigate the impact of vacuum gap distances on the performance of this TR configuration. As anticipated, as the vacuum gap distances increase from 50 nm to 1 μm, the maximum output power drastically decreases from 32.1 W/m^2 to 0.89 W/m^2. The maximum efficiency exhibits the same trend, decreasing from 33% to 20%, emphasizing the critical importance of maintaining a nanoscale vacuum gap distance for the performance of this concentrated near-field TR configuration. If the gap distance further increases, the polar dielectric may not be an optimal absorber, as the surface modes would no longer dominate the radiative heat transfer. The optimal emitter temperature decreases as the photon extraction process becomes less selective and the dissipated power becomes less efficient with increasing gap distance. Without the near-field effect, fewer useful photons (with energy close to and above the bandgap) are emitted into the cold space, leading to a deterioration in performance. To highlight the importance of the near-field effect, we simulated a far-field case using a blackbody absorber and an ideal emitter. The results showed limited performance improvement (Figure S3), underscoring that the near-field absorber's key advantage is its selective narrow-band enhancement of photon extraction above the bandgap.

Further Optimizations and Perspectives. We utilized both gradient-based algorithms and genetic algorithms to explore the optimal material properties of the polar dielectric. However, given the complex and nonlinear solution space, neither algorithm can guarantee that the optimal point is the global optimum. The provided parameter set for the polar dielectric is the optimal result from multiple initial starting points. Due to computational constraints, we only try to optimize the values of ω_{TO}, ω_{LO}, and γ with the rest parameters fixed (see Methods). In essence, these results may not fully unveil the best potential for this concentrated near-field TR configuration, and additional design and optimization efforts could further enhance its performance, as discussed in the Supporting Information. Simultaneously, to ensure the practical implementation of this high-performance configuration, additional engineering considerations are necessary. When optimizing the thickness of the polar dielectric absorber and the radiative cooling emitter, efforts should be made to minimize contact thermal resistance resulting from interfaces or thermal leakage from the environment. A vacuum chamber, featuring a transparent shield on top, should enclose the entire configuration to minimize the impact of convection.[48] The MCT material must exhibit high quality to ensure quantum efficiency and minimize nonradiative loss. The consideration of nonradiative processes and electrical loss may reduce the performance of narrow bandgap semiconductor devices.[13,49−51] However, the structure of this MCT TR device and electrical circuit design can be further optimized to suppress nonradiative losses and minimize transport losses.[52]

The material selection and integration are the next questions in realizing the concentrated near-field TR device. Based on the optimization of the absorber, polar dielectrics with optical phonon frequencies around the optimal bandgap, such as SiO_2, $BaSO_4$, and SiC, are potentially good candidates to extract photons from the TR cell. However, these materials in the film structure are not optimal for the radiative cooling emitter as their Reststrahlen band also falls directly on the sky window, significantly suppressing far-field thermal radiation. Interestingly, in particle form, these materials serve as excellent emission centers for radiative cooling film and paint.[24,25,28] Therefore, it is possible to use a single material to develop both the polar dielectric absorber and radiative cooling emitter. Using a concentrated radiative cooling emitter made from affordable nanocomposite materials would be a more cost-effective way to harness the thermal power of the night sky, compared to deploying expensive TR cells made of semiconductors. Another essential component for a high-performance concentrated near-field atmosphere coupler is a good heat spreader, capable of uniformly distributing heat from a small area to a larger surface. In addition to the concentrated near-field atmosphere coupler, a far-field thermal radiation extractor made of high-refractive-index material could be employed to enhance dissipated power within optical limits.[53,54] A straightforward improvement to the current design is to integrate this far-field thermal radiation extractor with the ideal emitter to minimize Fresnel reflection loss at the emitter−air interface.

While there are challenges to prototyping this proposed design, it is crucial to emphasize that this type of nighttime power generator is inherently antiglobal warming compared to other conventional power generation methods. According to the second law of thermodynamics, waste heat is inevitable in power generation. The more inefficient the power generator is, the more heat is released into the Earth's environment, contributing to global warming. This is a key factor in the impact of human activity on the Earth's environment. Furthermore, since the heat source for this nighttime power generation is derived from waste heat, no additional fossil fuel consumption is necessary. Consequently, nighttime power generation emerges as a unique

https://doi.org/10.1021/acsnano.4c16433
ACS Nano 2025, 19, 17357−17364

and environmentally conscious technology, acting as a countermeasure against global warming.

CONCLUSIONS

In summary, we proposed a concentrated near-field TR device capable of generating output power comparable to a solar panel. The novel aspect of this technology lies in the incorporation of a concentrated near-field coupler positioned between the TR cell and deep space, which significantly enhances the photon and heat transfer from the hot to cold reservoir, resulting in enhanced performance. This underscores the substantial potential of TR technology to achieve outputs exceeding 1 W/m^2 with decent efficiency, surpassing current experimental benchmarks. Drawing parallels to the advancements seen in concentrated solar power within the solar power technology landscape, we anticipate that this research initiative will pave the way for the development of nighttime power generation and expedite the realization and potentially the commercialization of TR technology, positioning it as a vital technology in renewable energy generation.

METHODS

Material Properties of the Polar Dielectric and $Hg_xCd_{1-x}Te$. The dielectric function of the polar dielectric absorber is modeled by the Lorentz oscillator model

$$\varepsilon_{pd}(\omega) = \varepsilon_\infty\left(1 + \frac{\omega_g^2 r_{TO}^2 r_{LO}^2 - \omega_g^2 r_{TO}^2}{\omega_g^2 r_{TO}^2 - \omega^2 - i\omega\omega_g r_\gamma}\right) \tag{1}$$

where ε_∞ is the dielectric constant at the high-frequency limit, and ω is the angular frequency. $r_{TO} = \omega_{TO}/\omega_g$ and $r_{LO} = \omega_{LO}/\omega_g$, where ω_{TO} and ω_{LO} are the frequencies of the transverse and longitudinal optical phonon at the zone center, respectively. $r_\gamma = \gamma/\omega_g$, where γ is the damping factor. In this way, the parameters of the Lorentz oscillator model are normalized to ω_g, which is easy for optimization of the polar dielectric absorber. $\omega_g = E_g/\hbar$ is the frequency of the bandgap of $Hg_xCd_{1-x}Te$ (MCT), which is given by eq 8 in ref 55. The dielectric function of MCT is calculated by $\varepsilon_{MCT}(\omega) = (n + i\kappa)^2$, where $i = \sqrt{-1}$, n is the refractive index, which is fitted by the experimental data in ref 56, and κ is the extinction coefficient, which is calculated by the absorption coefficient.[14,55]

Detailed Balance Analysis. The detailed balance analysis is used to calculate the current density of the conventional thermoradiative (TR) cell

$$J(V) = \frac{e}{2\pi^2 c^2}\int_{\omega_g}^{\infty}\int_0^{\pi/2} E_{TR}(\omega, \theta)A_a(\omega, \theta)\omega^2 [\psi(\omega, T_h, V) - \Theta(\omega, T_c)]\sin(\theta)\cos(\theta)\, d\theta\, d\omega \tag{2}$$

where c is the speed of light, e is the elementary charge, and θ is the zenith angle. The effect of the azimuth angle has been included as a constant of 2π. $\Theta(\omega, T) = [\exp(\hbar\omega/k_BT) - 1]^{-1}$ is the Bose−Einstein distribution, and $\psi(\omega, T, V) = \{\exp[(\hbar\omega - Ve)/k_BT] - 1\}^{-1}$ is modified Bose−Einstein distribution with a given photon chemical potential of Ve.[57,58] $E_{TR}(\omega,\theta)$ is the spectral directional emissivity of the TR cell.[14,59] $A_a(\omega,\theta) = 1 - Tr_a(\omega)^{1/\cos(\theta)}$ is the spectral directional absorptivity of the atmosphere, and $Tr_a(\omega)$ is the spectral transitivity of the atmosphere.[43] The expression to calculate the dissipated power is very similar to that of the current density

$$Q_c(V) = \frac{1}{2\pi^2 c^2}\int_0^{\infty}\int_0^{\pi/2} E_{TR}(\omega, \theta)A_a(\omega, \theta)\hbar\omega^3 [\psi(\omega, T_h, V) - \Theta(\omega, T_c)]\sin(\theta)\cos(\theta)\, d\theta\, d\omega \tag{3}$$

where $\hbar$ is the reduced Planck constant. The output power per unit area and conversion efficiency are obtained by

$$P(V) = J(V)V \tag{4}$$

And

$$\eta(V) = \frac{P(V)}{Q_c(V) + P(V)} \tag{5}$$

Near-Field Thermoradiative Cell. A fluctuational electrodynamic formula is used to calculate the current density of the near-field TR cell.[13,14,60]

$$J(V) = \frac{e}{4\pi^2}\int_{\omega_g}^{\infty}[\psi(\omega, T_h, V) - \Theta(\omega, T_e)]\, d\omega \int_0^{\infty}\sum_{m=s,p}\xi_j(\omega, k_\parallel)k_\parallel\, dk_\parallel \tag{6}$$

where $\xi_j(\omega,k_\parallel)$ represents the energy transmission coefficient from the MCT TR cell to the upper region (the polar dielectric absorber and air at the top), and the subscript j represents either the transverse electric waves (s-polarization) or transverse magnetic waves (p-polarization). $k_\parallel = \sqrt{k_x^2 + k_y^2}$ is the magnitude of the parallel wavevector in the $x-y$ plane. The energy transmission coefficient can be obtained with a recursive transfer matrix method[13,14,60]

$$\xi_j(\omega, k_\parallel) = \int_0^{t_{TR}} \mathrm{Re}[i\varepsilon''_{MCT}F(\omega, k_\parallel, z, t_{TR})]\, dz \tag{7}$$

The function F represents the general solution of the multilayer Green function for the emission at the position of t_{TR} generated from the position z, and ε''_{MCT} is the imaginary part of the dielectric functions of MCT. The net heat flux between the TR cell and the polar dielectric absorber can be expressed similarly

$$Q_c(V) = \frac{\hbar}{4\pi^2}\int_0^{\infty}[\psi(\omega, T_h, V) - \Theta(\omega, T_e)]\omega\, d\omega \int_0^{\infty}\sum_{m=s,p}\xi_j(\omega, k_\parallel)k_\parallel\, dk_\parallel \tag{8}$$

The calculations of the output power and efficiency can be simply done by substituting eqs 6 and 8 into eqs 4 and 5.

Optimization of the Polar Dielectric Absorber. We try to find the best polar dielectric with one oscillator with maximum output power or efficiency by solving a constrained optimization problem. Here, we fixed the dielectric constant ($\varepsilon_\infty = 7$) and the bandgap ($E_g = 0.094$ eV) of MCT, geometric structures ($t_{pd} = 1\ \mu$m, $t_{TR} = 50$ nm, $d = 10$ nm), and temperature difference ($T_h = 300$ K and $T_e = 290$ K) due to computational cost. The optimization problem is set up

$$\text{maximize } \eta(r_{TO}, r_{LO}, r_\gamma) \tag{9}$$

$$\begin{aligned} \textit{subject to}\quad & 0.5 \le r_{TO} \le 1.8 \\ & 1.001 \le r_{LO} \le 2 \\ & 0.0001 \le r_\gamma \le 1 \end{aligned} \tag{10}$$

The constraints for r_{TO}, r_{LO}, and r_γ aim to concentrate the emission from the TR cell close to the bandgap, maximizing the performance of the TR cell. The objective function has been set up to maximize the conversion efficiency. Both results have been shown in Figure S4. We employ both the interior point method and the genetic algorithm to search for the optimum. However, considering the complex and wavy nature of the solution space, multiple initial points are chosen to enhance the likelihood of finding the global optimum. Due to the computational cost, we choose the polar dielectric to be $r_{TO} = 1.0867$, $r_{TO} = 1.2669$, and $r_\gamma = 0.0035$. Note that this result is optimal after 10 runs, but it is not guaranteed as the global optimum.

Ideal Thermal Emitter at Nighttime. The maximum emissive power of the thermal emitter can be obtained by

https://doi.org/10.1021/acsnano.4c16433
ACS Nano 2025, 19, 17357−17364

$$Q_e(T_e) = \frac{1}{2\pi^2 c^2}\int_0^\infty \int_0^{\pi/2} E(\omega, \theta, T_e)A_a(\omega, \theta)\hbar\omega^3 [\Theta(\omega, T_e) - \Theta(\omega, T_c)]\sin(\theta)\cos(\theta)\, d\theta\, d\omega \quad (11)$$

where E is the emissivity of a thermal emitter. To design the ideal thermal emitter at nighttime, we have to consider the transmissivity of the atmosphere and the environment radiation leakage. The criterion is that if the outgoing directional spectral heat flux at a specific angle and surface temperature is larger than the incoming directional spectral heat flux, we set the emissivity to be unity. Otherwise, it is set to zero. Therefore, the directional spectral emissivity of an ideal thermal emitter at nighttime is given by

$$E_{ideal}(\omega, \theta, T_e) = \begin{cases} 1, & q_{out}(\omega, \theta, T_e) > q_{in}(\omega, \theta, T_e) \\ 0, & q_{out}(\omega, \theta, T_e) \le q_{in}(\omega, \theta, T_e) \end{cases} \quad (12)$$

where q_{out} and q_{in} represent the outgoing thermal radiation through the atmosphere and heat leakage from the environment, respectively. They are obtained by

$$q_{out}(\omega, \theta, T_e) = [1 - A_a(\omega, \theta)](\Theta(\omega, T_e) - \Theta(\omega, T_c)) \quad (13)$$

And

$$q_{in}(\omega, \theta, T_e) = A_a(\omega, \theta)(\Theta(\omega, T_a) - \Theta(\omega, T_e)) \quad (14)$$

The detailed spectral emissivity can be found in Figure S5.

ASSOCIATED CONTENT

Data Availability Statement

The code used to compute the device performance is available from the corresponding authors upon reasonable request.

Supporting Information

The Supporting Information is available free of charge at https://pubs.acs.org/doi/10.1021/acsnano.4c16433.

Detailed discussions, including the performance of the concentrated near-field TR configuration using a blackbody emitter and a ultrawhite radiative cooling paint, concentrated far-field TR configuration with a blackbody absorber and an ideal emitter, optimization of the polar dielectric absorber, and ideal spectrum of a thermal emitter (PDF)

AUTHOR INFORMATION

Corresponding Authors

Dudong Feng − *School of Mechanical Engineering and the Birck Nanotechnology Center, Purdue University, West Lafayette, Indiana 47907-2088, United States;* orcid.org/0000-0002-2289-1313; Email: fengdudong@purdue.edu

Xiulin Ruan − *School of Mechanical Engineering and the Birck Nanotechnology Center, Purdue University, West Lafayette, Indiana 47907-2088, United States;* orcid.org/0000-0001-7611-7449; Email: ruan@purdue.edu

Complete contact information is available at: https://pubs.acs.org/10.1021/acsnano.4c16433

Author Contributions

X.R. and D.F. conceptualized the idea; D.F. performed the majority of the calculations, analyzed the data, and wrote the draft paper; X.R. and D.F. edited the paper; X.R. supervised the work.

Notes

The authors declare the following competing financial interest(s): X.R. and D.F. are co-inventors of a provisional patent based on this work being prepared to be filed with the U.S. Patent and Trademark Office.

ACKNOWLEDGMENTS

D.F. and X.R. acknowledge partial support from the US National Science Foundation through award 2102645.

REFERENCES

(1) Green, M. A. *Third Generation Photovoltaics*; Springer Nature, 2006.

(2) Xu, Z.; Li, Y.; Gao, G.; Xie, F.; Ju, R.; Yu, S.; Liu, K.; Li, J.; Wang, W.; Li, W.; Li, T.; Qiu, C.-W. Scalable selective absorber with quasiperiodic nanostructure for low-grade solar energy harvesting. *APL Photonics* **2023**, *8* (2), 020801.

(3) Lord, S. D. *A New Software Tool for Computing Earth's Atmospheric Transmission of Near- and Far-Infrared Radiation*. 103957; Ames Research Center, 1992.

(4) Peixoto, J. P.; Oort, A. H. *Physics of Climate*; American Institute of Physics: New York, NY, 1992; p 520.

(5) Buddhiraju, S.; Santhanam, P.; Fan, S. Thermodynamic limits of energy harvesting from outgoing thermal radiation. *Proc. Natl. Acad. Sci. U.S.A.* **2018**, *115* (16), E3609−E3615.

(6) Byrnes, S. J.; Blanchard, R.; Capasso, F. Harvesting renewable energy from Earth's mid-infrared emissions. *Proc. Natl. Acad. Sci. U.S.A.* **2014**, *111* (11), 3927−3932.

(7) Strandberg, R. Heat to electricity conversion by cold carrier emissive energy harvesters. *J. Appl. Phys.* **2015**, *118* (21), 215102.

(8) Strandberg, R. Theoretical efficiency limits for thermoradiative energy conversion. *J. Appl. Phys.* **2015**, *117* (5), 055105.

(9) Short, W.; Packey, D.; Holt, T. *A Manual for the Economic Evaluation of Energy Efficiency and Renewable Energy Technologies*; National Renewable Energy Laboratory, 1995.

(10) Timilsina, G. R.; Kurdgelashvili, L.; Narbel, P. A. Solar energy: Markets, economics and policies. *Renewable Sustainable Energy Rev.* **2012**, *16* (1), 449−465.

(11) Loeb, N. G.; Johnson, G. C.; Thorsen, T. J.; Lyman, J. M.; Rose, F. G.; Kato, S. Satellite and Ocean Data Reveal Marked Increase in Earth's Heating Rate. *Geophys. Res. Lett.* **2021**, *48* (13), No. e2021GL093047.

(12) Santhanam, P.; Fan, S. Thermal-to-electrical energy conversion by diodes under negative illumination. *Phys. Rev. B* **2016**, *93* (16), 161410.

(13) Feng, D.; Ruan, X.; Yee, S. K.; Zhang, Z. M. Thermoradiative devices enabled by hyperbolic phonon polaritons at nanoscales. *Nano Energy* **2022**, *103*, 107831.

(14) Zhang, Z. M. *Nano/Microscale Heat Transfer*; Springer Nature, 2020.

(15) Ono, M.; Santhanam, P.; Li, W.; Zhao, B.; Fan, S. Experimental demonstration of energy harvesting from the sky using the negative illumination effect of a semiconductor photodiode. *Appl. Phys. Lett.* **2019**, *114* (16), 161102.

(16) Nielsen, M. P.; Pusch, A.; Sazzad, M. H.; Pearce, P. M.; Reece, P. J.; Ekins-Daukes, N. J. Thermoradiative Power Conversion from HgCdTe Photodiodes and Their Current−Voltage Characteristics. *ACS Photonics* **2022**, *9* (5), 1535−1540.

(17) Harrison, A. W.; Walton, M. R. Radiative cooling of TiO2 white paint. *Sol. Energy* **1978**, *20* (2), 185−188.

(18) Eriksson, T. S.; Lushiku, E. M.; Granqvist, C. G. Materials for radiative cooling to low temperature. *Sol. Energy Mater.* **1984**, *11* (3), 149−161.

(19) Lushiku, E. M.; Granqvist, C.-G. Radiative cooling with selectively infrared-emitting gases. *Appl. Opt.* **1984**, *23* (11), 1835−1843.

(20) Eriksson, T. S.; Granqvist, C. G. Radiative cooling computed for model atmospheres. *Appl. Opt.* **1982**, *21* (23), 4381−4388.

(21) Lushiku, E. M.; Hjortsberg, A.; Granqvist, C. G. Radiative cooling with selectively infrared-emitting ammonia gas. *J. Appl. Phys.* **1982**, *53* (8), 5526−5530.

(22) Granqvist, C. G.; Hjortsberg, A. Radiative cooling to low temperatures: General considerations and application to selectively emitting SiO films. *J. Appl. Phys.* **1981**, *52* (6), 4205−4220.
(23) Catalanotti, S.; Cuomo, V.; Piro, G.; Ruggi, D.; Silvestrini, V.; Troise, G. The radiative cooling of selective surfaces. *Sol. Energy* **1975**, *17* (2), 83−89.
(24) Fan, S.; Li, W. Photonics and thermodynamics concepts in radiative cooling. *Nat. Photonics* **2022**, *16* (3), 182−190.
(25) Li, X.; Peoples, J.; Yao, P.; Ruan, X. Ultrawhite BaSO4 Paints and Films for Remarkable Daytime Subambient Radiative Cooling. *ACS Appl. Mater. Interfaces* **2021**, *13* (18), 21733−21739.
(26) Li, D.; Liu, X.; Li, W.; Lin, Z.; Zhu, B.; Li, Z.; Li, J.; Li, B.; Fan, S.; Xie, J.; Zhu, J. Scalable and hierarchically designed polymer film as a selective thermal emitter for high-performance all-day radiative cooling. *Nat. Nanotechnol.* **2021**, *16* (2), 153−158.
(27) Zhu, B.; Li, W.; Zhang, Q.; Li, D.; Liu, X.; Wang, Y.; Xu, N.; Wu, Z.; Li, J.; Li, X.; Catrysse, P. B.; Xu, W.; Fan, S.; Zhu, J. Subambient daytime radiative cooling textile based on nanoprocessed silk. *Nat. Nanotechnol.* **2021**, *16* (12), 1342−1348.
(28) Li, X.; Peoples, J.; Huang, Z.; Zhao, Z.; Qiu, J.; Ruan, X. Full Daytime Sub-ambient Radiative Cooling in Commercial-like Paints with High Figure of Merit. *Cell Rep. Phys. Sci.* **2020**, *1* (10), 100221.
(29) Yang, P.; Chen, C.; Zhang, Z. M. A dual-layer structure with record-high solar reflectance for daytime radiative cooling. *Sol. Energy* **2018**, *169*, 316−324.
(30) Zhai, Y.; Ma, Y.; David, S. N.; Zhao, D.; Lou, R.; Tan, G.; Yang, R.; Yin, X. Scalable-manufactured randomized glass-polymer hybrid metamaterial for daytime radiative cooling. *Science* **2017**, *355* (6329), 1062−1066.
(31) Raman, A. P.; Anoma, M. A.; Zhu, L.; Rephaeli, E.; Fan, S. Passive radiative cooling below ambient air temperature under direct sunlight. *Nature* **2014**, *515* (7528), 540−544.
(32) Liao, T.; Xu, Q.; Dai, Y.; Cheng, C.; He, Q.; Ni, M. Radiative cooling-assisted thermoelectric refrigeration and power systems: Coupling properties and parametric optimization. *Energy* **2022**, *242*, 122546.
(33) Raman, A. P.; Li, W.; Fan, S. Generating Light from Darkness. *Joule* **2019**, *3* (11), 2679−2686.
(34) Khan, S.; Kim, J.; Roh, K.; Park, G.; Kim, W. High power density of radiative-cooled compact thermoelectric generator based on body heat harvesting. *Nano Energy* **2021**, *87*, 106180.
(35) Yu, L.; Xi, Z.; Li, S.; Pang, D.; Yan, H.; Chen, M. All-day continuous electrical power generator by solar heating and radiative cooling from the sky. *Appl. Energy* **2022**, *322*, 119403.
(36) Assawaworrarit, S.; Omair, Z.; Fan, S. Nighttime electric power generation at a density of 50 mW/m2 via radiative cooling of a photovoltaic cell. *Appl. Phys. Lett.* **2022**, *120* (14), 143901.
(37) Omair, Z.; Assawaworrarit, S.; Fan, L.; Jin, W.; Fan, S. Radiative-cooling-based nighttime electricity generation with power density exceeding 100 mW/m2. *iScience* **2022**, *25* (8), 104858.
(38) Fan, L.; Li, W.; Jin, W.; Orenstein, M.; Fan, S. Maximal nighttime electrical power generation via optimal radiative cooling. *Opt. Express* **2020**, *28* (17), 25460−25470.
(39) Feng, D.; Yang, X.; Ruan, X. Phonon Scattering Engineered Unconventional Thermal Radiation at the Nanoscale. *Nano Lett.* **2023**, *23* (21), 10044−10050.
(40) Feng, D.; Yang, X.; Han, Z.; Ruan, X. Near-field radiation in BAs and BSb dominated by four-phonon scattering. *Phys. Rev. B* **2024**, *109* (8), L081409.
(41) Feng, D.; Yee, S. K.; Zhang, Z. M. Near-field photonic thermal diode based on hBN and InSb films. *Appl. Phys. Lett.* **2021**, *119* (18), 181111.
(42) Li, L.; Yu, K.; Feng, D.; Yang, Z.; Zhang, K.; Liu, Y.; Wu, X. High-performance near-field thermophotovoltaics based on a ${\mathrm{Ca}\mathrm{CO}}_{3}/\mathrm{graphene}/\mathrm{In}\mathrm{Sb}$ heterostructure. *Phys. Rev. Appl.* **2023**, *20* (6), 064015.
(43) R Transmission Spectra Gemini Observatory. https://www.gemini.edu/observing/telescopes-and-sites/sites#Transmission (accessed April 15).
(44) Dong, M.; Zhu, L.; Jiang, B.; Fan, S.; Chen, Z. Concentrated radiative cooling and its constraint from reciprocity. *Opt. Express* **2022**, *30* (1), 275−285.
(45) Zhou, L.; Song, H.; Zhang, N.; Rada, J.; Singer, M.; Zhang, H.; Ooi, B. S.; Yu, Z.; Gan, Q. Hybrid concentrated radiative cooling and solar heating in a single system. *Cell Rep. Phys. Sci.* **2021**, *2* (2), 100338.
(46) Peoples, J.; Hung, Y.-W.; Li, X.; Gallagher, D.; Fruehe, N.; Pottschmidt, M.; Breseman, C.; Adams, C.; Yuksel, A.; Braun, J.; Horton, W. T.; Ruan, X. Concentrated radiative cooling. *Appl. Energy* **2022**, *310*, 118368.
(47) Kraemer, D.; Poudel, B.; Feng, H.-P.; Caylor, J. C.; Yu, B.; Yan, X.; Ma, Y.; Wang, X.; Wang, D.; Muto, A.; McEnaney, K.; Chiesa, M.; Ren, Z.; Chen, G. High-performance flat-panel solar thermoelectric generators with high thermal concentration. *Nat. Mater.* **2011**, *10* (7), 532−538.
(48) Chen, Z.; Zhu, L.; Raman, A.; Fan, S. Radiative cooling to deep sub-freezing temperatures through a 24-h day−night cycle. *Nat. Commun.* **2016**, *7* (1), 13729.
(49) Feng, D.; Tervo, E. J.; Vasileska, D.; Yee, S. K.; Rohatgi, A.; Zhang, Z. M. Spatial profiles of photon chemical potential in near-field thermophotovoltaic cells. *J. Appl. Phys.* **2021**, *129* (21), 213101.
(50) Feng, D.; Yee, S. K.; Zhang, Z. M. Improved performance of a near-field thermophotovoltaic device by a back gapped reflector. *Sol. Energy Mater. Sol. Cells* **2022**, *237*, 111562.
(51) Callahan, W. A.; Feng, D.; Zhang, Z. M.; Toberer, E. S.; Ferguson, A. J.; Tervo, E. J. Coupled Charge and Radiation Transport Processes in Thermophotovoltaic and Thermoradiative Cells. *Phys. Rev. Appl.* **2021**, *15* (5), 054035.
(52) Pidgeon, C. R.; Ciesla, C. M.; Murdin, B. N. Suppression of non-radiative processes in semiconductor mid-infrared emitters and detectors. *Prog. Quantum Electron.* **1997**, *21* (5), 361−419.
(53) Yu, Z.; Sergeant, N. P.; Skauli, T.; Zhang, G.; Wang, H.; Fan, S. Enhancing far-field thermal emission with thermal extraction. *Nat. Commun.* **2013**, *4* (1), 1730.
(54) Tan, Y.; Liu, B.; Shen, S.; Yu, Z. Enhancing radiative energy transfer through thermal extraction. *Nanophotonics* **2016**, *5* (1), 22−30.
(55) Schacham, S. E.; Finkman, E. Recombination mechanisms in p-type HgCdTe: Freezeout and background flux effects. *J. Appl. Phys.* **1985**, *57* (6), 2001−2009.
(56) Kučera, Z. Dispersion of the refractive index of Hg1−xCdxTe. *Phys. Status Solidi A* **1987**, *100* (2), 659−665.
(57) Feng, D.; Tervo, E. J.; Yee, S. K.; Zhang, Z. M. Effect of Evanescent Waves on the Dark Current of Thermophotovoltaic Cells. *Nanoscale Microscale Thermophys. Eng.* **2020**, *24* (1), 1−19.
(58) Wurfel, P. The chemical potential of radiation. *J. Phys. C: Solid State Phys.* **1982**, *15* (18), 3967−3985.
(59) Feng, D.; Yee, S. K.; Zhang, Z. M. Geometric and doping effects on radiative recombination in thin-film near-field energy converters. *AIP Adv.* **2022**, *12* (9), 095006.
(60) Feng, D. *Study of the Photon Chemical Potential in Semiconductor Radiative Energy Converters at Micro/Nanoscales*. Ph. D. Thesis, Georgia Institute of Technology, 2021.

https://doi.org/10.1021/acsnano.4c16433
ACS Nano 2025, 19, 17357−17364